CO_2 uptake by accelerated carbonation of recycled concrete aggregates: characterization at the grain scale by tomography and micro-indentation

Farah KADDAH[1,2], Jérôme LUX[3], Emmanuel ROZIERE[2], Philippe TURCRY[3*], Ouali AMIRI[2], Harifidy RANAIVOMANANA[2], Abdelkarim AIT-MOKHTAR[3]

[1]Nantes Université, Ecole Centrale Nantes, CNRS, GeM, UMR 6183, F-44000 Nantes, France, emmanuel.roziere@ec-nantes.fr, harifidy.ranaivomanana@univ-nantes.fr, ouali.amiri@univ-nantes.fr

[2]Research and Innovation Center on CO_2 and H_2 (RICH Center), Khalifa University of Science and Technology, Abu Dhabi, United Arab Emirates, farahchloe.kaddah@ku.ac.ae

[3]La Rochelle Université, CNRS, Laboratoire des Sciences de l'Ingénieur pour l'Environnement (LaSIE), UMR 7356, La Rochelle, France, jerome.lux@univ-lr.fr, philippe.turcry@univ-lr.fr, (corresponding author), karim.ait-mokhtar@univ-lr.fr*

Abstract

Accelerated carbonation of recycled concrete aggregates (RCA) is one of the approaches considered to reduce the carbon footprint of construction. After crushing, RCA can be used to mineralize CO_2 when exposed to industrial gases. This paper presents the results of an experimental campaign on 'model' RCA - cement paste spheres of 15 and 20 mm in diameter - tested during carbonation using innovative techniques, i.e., micro-indentation and micro-tomography. The specimens were carbonated at 20°C, 65% relative humidity, and 3% CO_2, following a drying step at 40°C and subsequent storage at 20°C and 55% relative humidity. Both techniques confirm that carbonation is uniform. Under these experimental conditions, and for these grain sizes, CO_2 reactive transport was primarily controlled by the kinetics of chemical reactions rather than gas diffusion.

1 Introduction

The carbonation of recycled aggregates (RA) obtained by crushing demolition waste is one of the approaches considered to reduce the carbon footprint of concrete construction [1]. At the scale of RA stockpiles stored at the crushing platform, CO_2 binding occurs under atmospheric conditions for a few weeks before use. However, several studies have shown that the natural carbonation of a stockpile is slow [2] or even negligible [3]. To carbonate RA more efficiently, accelerated processes were proposed during the FastCarb French National Project [4]. In large-scale reactors (rotary drum or fluidized bed), RA were exposed for 1 hour to industrial gases with high CO_2 concentration. This treatment accelerates gas transfer and significantly increases the CO_2 sequestration. The amount of CO_2 bound in this way was between 5 to 30 kg per ton of RA, depending on the grain size. Note that 10 kg/ton represents approximately 10% of the CO_2 emissions associated with the production of one ton of concrete. However, the environmental impact assessments of these processes show that the return on investment strongly depends on the transport distance of RA to the treatment site [5]. The viability of such processes, therefore, depends on their actual efficiency, meaning the amount of CO_2 bound per unit of carbonated material. To maximize this efficiency, laboratory studies are necessary to identify key parameters and understand the reactive transfer phenomenon at the scale of a centimeter-sized grain.

The present study focuses on "model recycled aggregates" subjected to accelerated carbonation in the laboratory. The experiments were conducted on cement paste spheres of different diameters, 15 and 20 mm, that were characterized after different durations in the reactor using innovative techniques, namely micro-indentation and micro-tomography. The latter are still rarely used for carbonation studies [6,7]. Their advantage is to map the interior of the grains, providing access to their carbonation state. The characterization methods are presented in the following sections, and the consequences of preconditioning on carbonation are discussed.

2 Experimental program

2.1 Material, sample geometry, and carbonation protocol

Spherical cement paste samples were made using a CEM I 52.5 cement (Table 1). The latter has a density of 3.13 and a specific surface area of 3,900 cm²/g. The cement paste was prepared with a water-to-cement (w/c) ratio of 0.6.

Table 1: Chemical composition of the cement (%)

CaO	SiO_2	Al_2O_3	MgO	Fe_2O_3	SO_3	TiO_2	K_2O	Na_2	P_2O_3
63.70	19.60	4.50	3.90	2.30	2.60	0.20	0.70	0.13	0.20

Two specimen sizes (Ø = 15 and 20 mm) were prepared to study the influence of the diameter on the carbonation process. The specimens were removed from the rubber molds after 24 hours and then immersed in a tap water tank maintained at a temperature of 23 ± 1°C for 27 days.

After this curing period, a preconditioning step was carried out to reduce the water saturation degree and to facilitate gas diffusion. The samples were dried at 40°C for 7 days and then stored in a climate-controlled room at 20°C and 55% RH until their mass stabilized (mass variation of less than 0.05% over 3 days). At the end of this preconditioning, we assume that the cement paste has reached moisture equilibrium with the external environment. The spheres were then placed in a climate chamber connected to a CO_2 reservoir, maintained at a temperature of 20°C, with a relative humidity of 65±5% and a CO_2 concentration of 3±0.5%.

In the following, the spheres with diameters of 15 and 20 mm are referred to as PC15 and PC20, respectively. The measurement time points are named as follows: C1 (before preconditioning), C2 (after preconditioning), C3 (2 days of carbonation), C4 (3 days), C5 (4 days), C6 (14 days), C7 (22 days), C8 (47 days).

2.2 Characterization methods

2.2.1 Thermogravimetric Analysis (TGA)

Thermal analysis was performed using a NETZSCH microbalance. For each characterization time, a sphere was crushed and sieved to 80 µm. A sample of approximately 100 mg was taken from the sieved material, placed in an alumina crucible, and suspended in the balance. The sample was heated at a rate of 10°C per minute under a nitrogen flow, from 20°C to 1000°C. The mass loss associated with decarbonation was determined by the mass difference between two temperatures defined by the boundaries of the characteristic peaks on the DTG curve (approximately between 500°C and 900°C).

2.2.2 Micro-indentation

A Fischer digital micro-hardness tester (FISCHERSCOPE HM2000) was used to evaluate the surface hardness of paste samples. At each characterization time, a sphere was cut in half, and one of the resulting hemispheres was subjected to the micro-indentation test. Before the test, the hemisphere was carefully polished to meet the experimental requirements of the tester. Initially positioned at the center of the hemisphere (X-coordinate = 0 mm), the indenter then moved toward the edge of the sample (X-coordinate = 7.5 or 10 mm). Along this linear trajectory, an indentation was made every 0.1 mm. For each indentation, a force of 300 N was applied for 10 seconds, and the depth reached by the indenter was measured to determine the hardness at that specific location. Each test gave us a microhardness profile.

2.2.3 Micro-tomography

Some PC15 and PC20 spheres were glued onto the supports shown in Fig. 1, prior to preconditioning, and underwent the entire protocol summarized in 2.1. At each time point Ci, the sphere and its support were imaged using micro-tomography with an XRADIA Micro XCT-400 device. The X-ray tube operated at 135 kV and 60 µA. A total of 1080 projections were acquired by the detector. Under these conditions, the resolution was approximately 10 µm (voxel edge size). This resolution was deemed sufficient to highlight density variations due to carbonation. The resulting images were 2048^3 in size, coded in 16 bits, totaling approximately 17 GB. The processing of grayscale histogram data is presented in Section III.B.

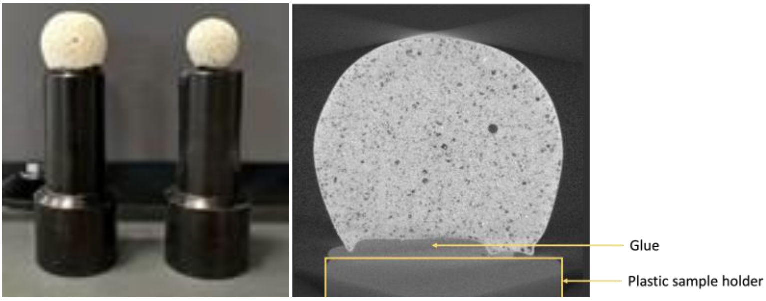

Fig. 1 View of the spheres glued to the supports used for tomography (left) and a cross-section of a 20 mm diameter sphere obtained by tomography (right).

3 Results

3.1 Mass evolution and CO_2 binding

Drying at 40°C followed by storage at 20°C for a total of 20 days leads to a mass loss of about 20%, corresponding to an average water saturation degree of the spheres of 30% (Fig. 2 Mass variations during preconditioning treatment (drying at 40°C, storage at 20°C), and accelerated carbonation). The mass variations were almost identical for both sizes during the preconditioning phase. Similarly, during the carbonation phase, from day 20 to day 48, the relative mass gain associated with CO_2 fixation did not depend on the diameter. This lack of size influence is primarily due to the spherical geometry. Furthermore, as discussed in the following, the same relative mass gain during carbonation for both diameters may indicate uniform carbonation.

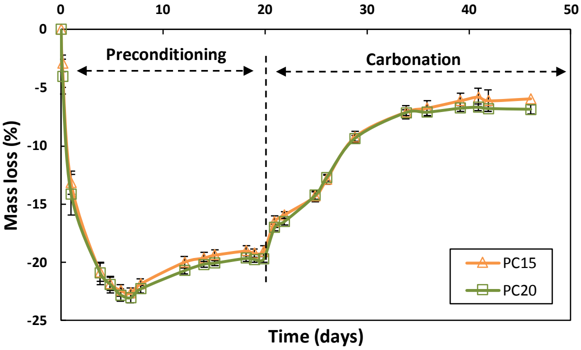

Fig. 2 Mass variations during preconditioning treatment (drying at 40°C, storage at 20°C), and accelerated carbonation

The results from the TGA confirm that the PC15 and PC20 spheres carbonate in the same way, as after 15 days, they have bound a total amount of about 250 g of CO_2 per kg of paste dried at 950°C (Fig. 3). It should be noted that the mass at 950°C serves as a reference because the material after LOI (loss on ignition) is fully dehydrated and decarbonated, thus remaining invariant during carbonation.

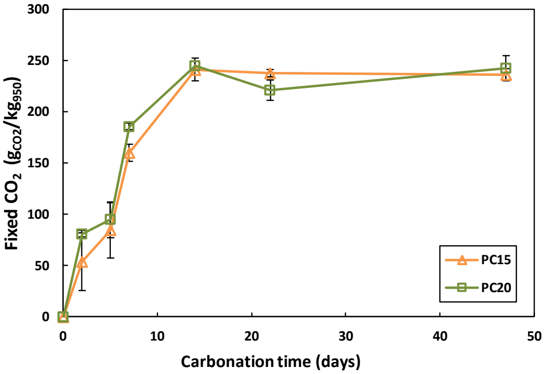

Fig. 3 Evolution of the amount of CO_2 bound by the spheres during carbonation determined by TGA.

3.2 Carbonation profiles

3.2.1 Micro-indentation

The hardness profiles were not affected by preconditioning (Fig. 4). However, the hardness significantly increased during carbonation, doubling on average after 14 days in the carbonation chamber. This increase is due to the higher hardness of calcium carbonates compared to hydrates such as C-S-H.

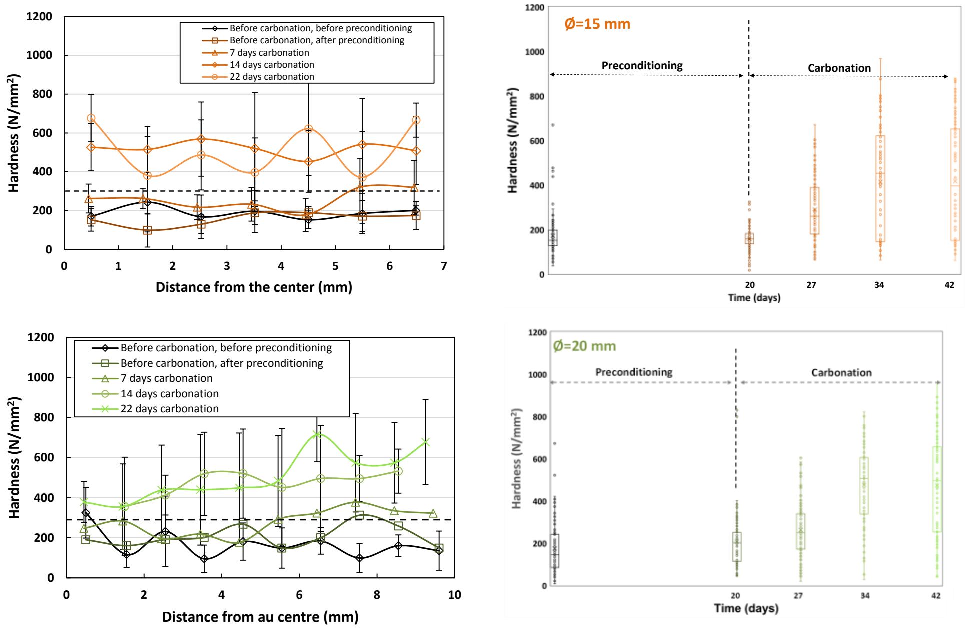

Fig. 4 Hardness profiles (left) and hardness values in the spheres at different times (right) for the two sizes: Ø = 15 mm at the top and Ø = 20 mm at the bottom.

In Fig. 4 (right), the time-dependent results clearly show that, while the average hardness increases, the results dispersion also grows during carbonation. The indenter moved along a straight line every 0.1 mm. The formation of calcium carbonates locally increases hardness, but the size of the newly formed minerals is smaller than the step size of the testing device. This also suggests incomplete carbonation of the paste. Additionally, the initial hardness dispersion is attributed to a hydration degree likely lower than 1 and the varying hardness of the paste constituents (hydrates, anhydrous phases).

The hardness profiles demonstrate uniform carbonation of the spheres after 14 days. There is very little difference between the average hardness at the surface and closer to the core. For the 20 mm diameter spheres, the profiles are slightly steeper, especially within the first 3 mm of the radius. The profiles corroborate the mass evolution and TGA results, as minimal changes were observed after 14 days of carbonation.

3.2.2 Tomography

X-ray tomography enables the reconstruction of a volume based on projections of the X-ray attenuation coefficients through a medium. During reconstruction, attenuation values are converted into grayscale levels (typically encoded as unsigned 16-bit integers) using a linear transformation that can differ for each image depending on the lower and upper values of the attenuation. In order to be able to make quantitative comparisons between different images, it is therefore necessary to transform the greyscale histograms so that the peaks which are a priori constant between the different time points (porosity or plastic support) are superimposed.

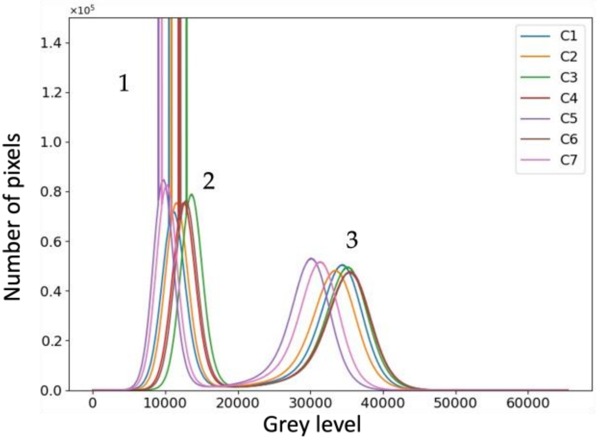

Fig. 5 Raw histograms of PC15 sample for all time points.

Fig 5 shows the raw histograms calculated for the PC15 sample image series. The three visible peaks correspond to: the grayscale level outside the field (constant background) (1), the porosity/external air peak (2), and the paste peak (3). Note that the peaks for the plastic sample holder and glue are not distinguishable due to the small number of voxels representing these phases compared to others. However, it is possible to detect the peak of the sample holder by restricting the analysis to a smaller subvolume. To rescale the grey-level histograms, we assumed that the grey-level peak corresponding to the air (P_0) and the peak of the plastic support (P_1) are constant from one term to the next. The alignment method involves calculating the gap between two reference peaks in an image and transforming the grayscale levels of other images to ensure that this gap remains constant. A translation was then applied to align one of the selected peaks to a fixed value, enabling comparison between images. The rescaled image $I'(\boldsymbol{x})$ can be computed as follows:

$$I'(\boldsymbol{x}) = a\, I(\boldsymbol{x}) + b$$

where: $a = \frac{P_1^{ref} - P_0^{ref}}{P_1 - P_0}$ and $b = C - aP_0$. P_0^{ref} and P_1^{ref} are the peak of air and sample holder determined on the first image respectively. C is the location of the rescaled porosity peak (here 10^5).

The precise determination of the peaks in histograms is carried out by a local maxima detection algorithm after a Gaussian filter with standard deviation σ = 4. The transformed images are then converted into 8-bit integers. Figure 6 shows the rescaled histograms for the PC15 sample.

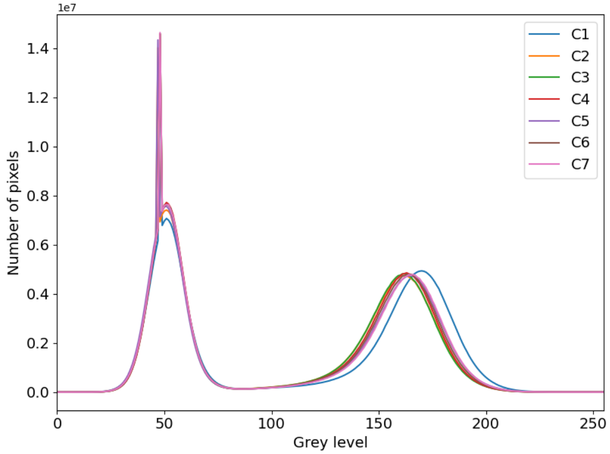

Fig. 6 Sub-volume (in yellow) used to determine the grayscale level peak of the plastic support (xz cut) (a) and histograms of the PC15 sample after alignment (b).

In order to carry out measurements on the series of images, it was necessary to differentiate the voxels that are inside *(the binary mask*) from those that are outside the sample. This was achieved by thresholding, followed by filtering (alternate sequential filtering with binary opening then binary closing) and pore filling. This binary mask is also used to calculate the distance map, which is an image whose voxel value represents the shortest distance to the background. Note that the bottom of the sample was assumed not to be in contact with the air.

Using both the binary mask and the distance map, it is possible to determine the evolution of greyscale dynamics as a function of the distance to the surface of the sample at different time points. Fig. 7 shows the evolution of the average grayscale level as a function of the distance to the sample surface. The greyscale levels were averaged in successive layers where the distance function is comprised between d_i and $d_i + \Delta d_i$.

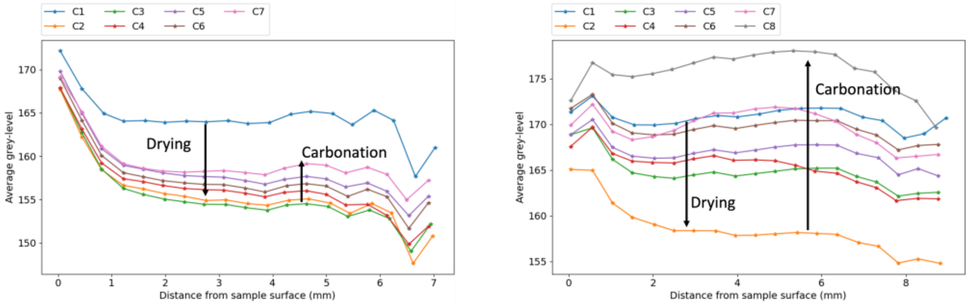

(a) (b)

Fig. 7 Evolution of the average grayscale level as a function of the distance from the sample surface, for all time points in PC15 (a) and PC20 (b) samples.

During the preconditioning phase, from time C1 to C2, the average grayscale levels decreased with the overall reduction in water content. For the two spheres with diameters of 15 mm and 20 mm, the grey-level profile remained unchanged, indicating a uniform evolution of the material. During carbonation, the average grayscale levels gradually increased, returning to the state before preconditioning (or even exceeding it, as seen at C8 after 47 days of carbonation for the PC20 sphere), indicating an increase in the average density within the sample. Again, the shape of the profiles did not change over time. From this, we deduced that the carbonation of the spheres was uniform. The profiles of the PC15 sphere show higher grayscale levels at the surface (within the first millimeter) from the beginning of preconditioning (C1). This profile shape is more challenging to interpret. The surface of the spheres may be denser due to wall effect and interface effects between the mold and the material during the first day after manufacturing. It is also possible that the cement hydration was better at the surface due to immersion in water during the 27 days of curing.

The size of one voxel side in the images being approximately 20 µm (after downsampling), it was impossible to segment the entire pore volume of the sample. Here, the choice was made to separate the voxels based on a threshold of 120, which visually corresponds to the resolved internal porosity, or at least to voxels containing more air than solid (Fig. 8). Note that this threshold corresponds to a deviation of approximately 3σ from the peak of the Gaussian that best approximates the solid peak of the driest sample (time C2). The time-evolution of the porosity segmented in this way as a function of the distance to the surface is shown in Fig. 9. During preconditioning, the so-defined porosity increased, which can be explained by a decrease in the water saturation of the pores visible in the image (larger than 20 µm), rather than a real increase in porosity. During carbonation, the segmented porosity tends to decrease, fairly uniformly within the spheres. This decrease can be interpreted as the formation of calcium carbonates, which tend to gradually fill the pores of the material during carbonation (hence an increase in grayscale levels). It should be noted that variations in water content during carbonation could also alter these grayscale profiles (as observed during preconditioning).

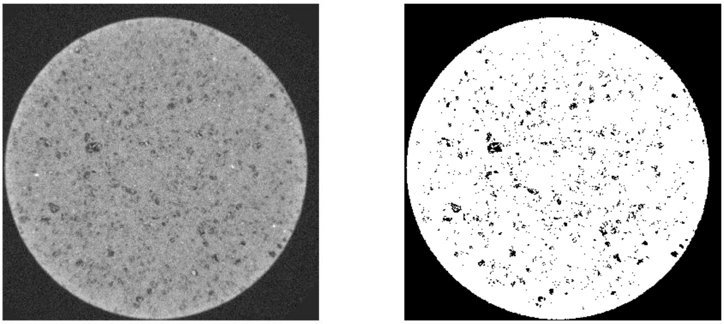

(a) (b)

Fig. 8 Cross-section of the PC15 sample at time C2 (a) and the binarized image (threshold 120) (b).

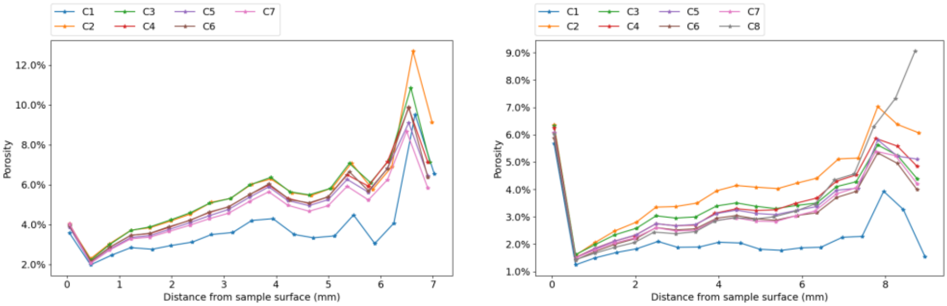

(a) (b)

Fig. 9 Evolution of the resolved porosity as a function of the distance from the sample surface, for all time points in PC15 (a) and PC20 (b) samples.

4 DISCUSSION

Micro-tomography and micro-indentation are well-suited techniques for obtaining profiles, which are difficult to determine at the aggregate scale using more traditional methods such as nibbling combined with TGA [8]. The first method allows for non-destructive monitoring of the same sample during carbonation. The main precaution to take is the presence of reference markers in the image to easily align grayscale histograms. Otherwise, image processing becomes complicated, and their interpretation is questionable. Micro-indentation is a destructive technique that requires several samples to be taken for time-based monitoring. A thorough preparation of the sample surfaces to be indented is also necessary. A more advanced processing of hardness profiles, based on the knowledge of each mineral's hardness, would allow for further analysis of the results.

In the study presented here, both techniques agree that carbonation occured almost uniformly for about 14 days, as suggested by the minimal differences in mass gain or CO_2 bound between the two diameters studied. The absence of a "carbonation front" allows us to propose a scenario regarding the reactive transfer of CO_2. For the low water saturation degree obtained after preconditioning, CO_2 diffuses rapidly and saturates the void volume of the aggregate before being consumed by the material. Unlike the classic scenario used for concrete structures, carbonation rate is not limited by gas diffusion but rather by chemical reactions.

5 CONCLUSION

Laboratory experiments on cement paste samples with spherical geometries were conducted to understand the carbonation phenomenon at the scale of a centimeter-sized recycled concrete aggregate. These experiments allowed us to test advanced characterization methods, namely micro-tomography and micro-indentation. Although they require careful preparation, data processing, and interpretation of results, these techniques proved well-suited for mapping carbonation inside the studied aggregates. These data are valuable as they confirm the result of numerical simulations from [9]: recycled aggregates in a relatively dry initial state (i.e., water saturation degree of about 30%) should carbonate uniformly, with the rate controlled by chemical reactions.

Acknowledgements

The authors thank the ANR for funding the CO_2NCRETE project. We also thank Mr. François Bertrand from the École Centrale de Nantes for performing the tomographic imaging.

References

[1] Habert, G., Miller, S.A., John, V.M., Provis, J.L., Favier, A., Horvath, A., and Scrivener K.L. 2020. “Environmental impacts and decarbonization strategies in the cement and concrete industries.” *Nature Review Earth & Environment* 1:559–573.

[2] Leemann, A., Münch, B., and Wyrzykowski, M. 2023. “CO2 absorption of recycled concrete aggregates in natural conditions.” *Materials Today Communications* 36.

[3] Hou, Y., Mahieux, P.Y., Turcry, Ph., Lux, J., and Aït-Mokhtar, A., and Nicolaï, A. 2022. “Plateforme de recyclage de déchets inertes du BTP : un puits de carbone « gris »?” *Academic Journal of Civil Engineering* 40(1): 96-99.

[4] Torrenti, J.M., Amiri, O., Barnes-Davin, L., Bougrain, F., Braymand, S., Cazacliu, B., Colin, J., Cudeville, A., Dangla, P., Djerbi, A., Doutreleau, M. Feraille, A., Gueguen, M., Guillot, X. Hou, Y., Izoret, L., Jacob, Y-P. Jeong, J., Lau Hiu Hoong, J. D., Mahieux, P-Y., Mai-Nhu, J., Martinez, H., Meyer, V., Morin, V., Pernin, T., Potier, J-M., Poulizac, L., Rougeau, P., Saadé, M., Schmitt, L., Sedran, T., Sereng, M., Soive, A., Symoes Dos Reys, G. Turcry, Ph. 2022. “The FastCarb project: Taking advantage of the accelerated carbonation of recycled concrete aggregates.” *Case Studies in Construction Materials* 17.

[5] Guyard, P., Saade, M., and Feraille, A. 2022. “Carbonatation accélérée de granulats de béton recyclés quels bénéfices environnementaux ?” *Academic Journal of Civil Engineering* 40(3): 117-131.

[6] D. Cui D, X. Zuo, K. Zheng, S. Talukdar. (2020). Tomography-Based Investigation on the Carbonation Behavior through the Surface-Opening Cracks of Sliced Paste Specimen. Materials, 13(8).

[7] Kaddah, F., Ranaivomanana, H., Amiri, O. and Rozière, E. 2022. “Accelerated carbonation of recycled concrete aggregates: Investigation on the microstructure and transport properties at cement paste and mortar scales,” *Journal of CO_2 Utilization* 57, 2022.

[8] Younsi, A., Turcry, Ph., Aït-Mokhtar, A. 2022. “Quantification of CO_2 uptake of concretes with mineral additions after 10-year natural carbonation.” *Journal of Cleaner Production* 349.

[9] Turcry, Ph., Huet, B., Mai-Nhu, J., Mahieux, P-Y., and Pernin, T. 2023. Modelling of the CO_2 uptake by recycled concrete aggregates. *The International RILEM Conference Synercrete*, Milos, Greece.